

MotionLCM: Real-time Controllable Motion Generation via Latent Consistency Model

Wenxun Dai¹, Ling-Hao Chen¹, Jingbo Wang^{2*}, Jinpeng Liu¹, Bo Dai^{2*}, Yansong Tang¹

¹Tsinghua University, ²Shanghai AI Laboratory

{wx dai2001, thu.lhchen, wangjingbo1219, liu.jinpeng.55}@gmail.com

{doubledaibo, tangyansong15}@gmail.com

Project page: <https://dai-wenxun.github.io/MotionLCM-page>

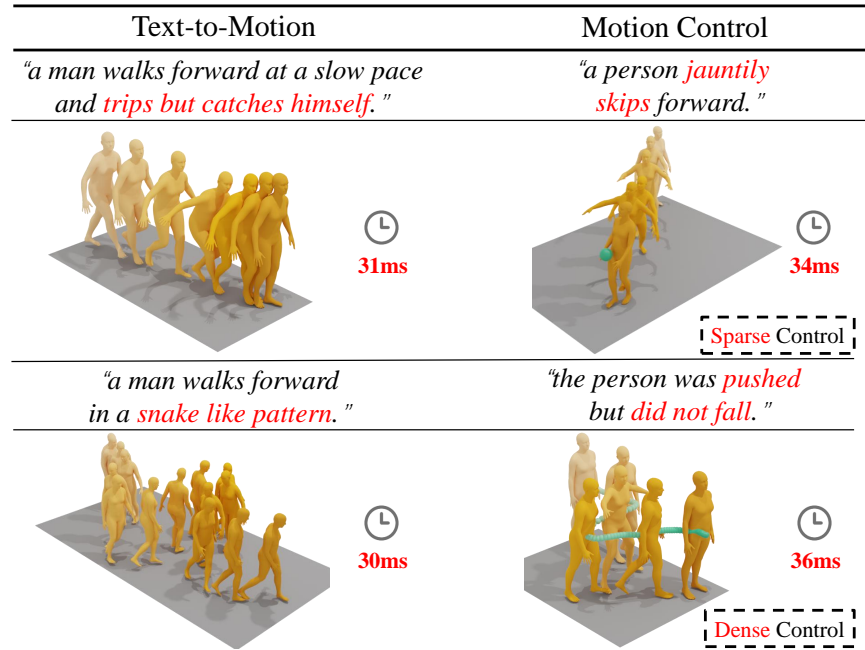


Figure 1: We propose MotionLCM, a real-time controllable motion latent consistency model, which is capable of achieving high-quality text-to-motion and precise motion control results (both sparse and dense conditions) in ~ 30 ms.

Abstract

This work introduces MotionLCM, extending controllable motion generation to a real-time level. Existing methods for spatial control in text-conditioned motion generation suffer from significant runtime inefficiency. To address this issue, we first propose the motion latent consistency model (MotionLCM) for motion generation, building upon the latent diffusion model [7] (MLD). By employing one-step (or few-step) inference, we further improve the runtime efficiency of the motion latent diffusion model for motion generation. To ensure effective controllability, we incorporate a motion ControlNet within the latent space of MotionLCM and enable explicit control signals (*e.g.*, pelvis trajectory) in the vanilla motion space to control the generation process directly, similar to controlling other latent-free diffusion models for motion generation [18]. By employing these techniques, our approach can generate human motions with text and control signals in real-time. Experimental results demonstrate the remarkable generation and controlling capabilities of MotionLCM while maintaining real-time runtime efficiency.

*Correspondence: Jingbo Wang and Bo Dai.

1 Introduction

Text-to-motion generation (T2M) has attracted increasing attention [1, 36, 47, 31, 12] due to its important roles in many applications [23, 51, 53]. Previous attempts mainly focus on GANs [1, 27], VAEs [15, 35, 36, 3] and diffusion models [7, 47, 60, 6, 8, 41, 58, 61, 28] via pairwise text-motion data [33, 13, 45, 37] and achieve impressive generation results. Existing approaches [47, 7, 60] mainly take diffusion models as a base generative model, owing to their powerful ability to model motion distribution. However, these diffusion fashions inevitably require considerable sampling steps for motion synthesis during inference, even with some sampling acceleration methods [43]. Specifically, MDM [47] and MLD [7] require $\sim 12s$ and $\sim 0.2s$ to generate a high-quality motion sequence. Such low efficiency blocks the applications of generating high-quality motions in various real-time scenarios.

In addition to the language description itself serving as a coarse control signal, another line of research focuses on controlling the motion generation with spatial constraints [41, 18, 54]. Although these attempts enjoy impressive controlling ability in the T2M task, there still exists a significant gap towards real-time applications. For example, based on MDM [47], OmniControl [54] exhibits a relatively long motion generation time, $\sim 72s$ per sequence. Therefore, trading-off between generation quality and efficiency is a challenging problem. As a result, in this paper, we target the real-time controllable motion generation research problem.

Recently, the concept of consistency models [44, 32] has been introduced in image generation, resulting in significant progress by enabling efficient and high-fidelity image synthesis with a minimal number of steps (e.g., 4 steps vs. 50 steps). These properties perfectly align with our goal of accelerating motion generation without compromising generation quality. As a result, we propose MotionLCM (Motion Latent Consistency Model) distilled by a motion latent diffusion model, MLD [7], to tackle the low-efficiency problem in diffusion sampling. To the best of our knowledge, we introduce consistency distillation into the motion generation area *for the first time* and accelerate motion generation to a real-time level via latent consistency distillation.

Here, in MotionLCM, we are facing another challenge on how to control motions with spatial signals (e.g., pelvis trajectory) in the latent space. Previous methods [54, 6, 41, 18] model human motions in the vanilla motion space and can manipulate the motion directly in the denoising process. However, for our latent-diffusion-based MotionLCM, it is non-trivial to feed the control signals into the latent space. This is because codes in the latent space have no explicit motion semantics, which cannot be manipulated directly by controlling signals. Inspired by the notable success of [59] in controllable image generation [40], we introduce a motion ControlNet to control motion generation in the latent space. However, the naïve motion ControlNet is not totally sufficient to provide supervision for controlling signals. The main reason is the lack of explicit supervision in the motion space. Therefore, during the training phase, we decode the predicted latent codes through the frozen VAE [20] decoder into vanilla motion space to provide explicit control supervision on the generated motion. Thanks to the powerful one-step inference capability of MotionLCM, the latent codes generated by MotionLCM can significantly facilitate control supervision both in the latent and motion space for training the motion ControlNet compared to MLD [7].

With our key designs, our proposed MotionLCM successfully enjoys the balance between the generation quality and efficiency in controllable motion generation. Before delivering into detail, we would like to sum up our core contributions as follows.

- We propose a Motion Latent Consistency Model (MotionLCM) via latent consistency distillation on the motion latent diffusion model extending controllable motion generation to a real-time level.

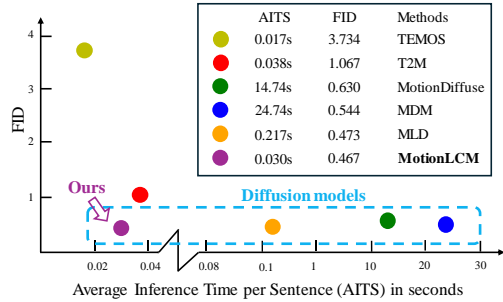


Figure 2: Comparison of the inference time costs on HumanML3D [13]. We compare the AITS and FID metrics with six SOTA methods. The closer the model is to the origin the better. Diffusion-based models are indicated by the blue dashed box. Our MotionLCM achieves real-time inference speed while ensuring high-quality motion generation.

- Building upon our achievement of real-time motion generation, we introduce a motion ControlNet, enabling high-quality controllable motion generation.
- Extensive experimental results show that MotionLCM enjoys a good balance of generation quality, controlling capability, and real-time efficiency.

2 Related Work

2.1 Human Motion Generation

Generating human motions can be divided into two main fashions according to inputs: motion synthesis 1) without any condition [57, 63, 62, 47, 39], and 2) with some given multi-modal conditions, such as action labels [10, 21, 35, 15, 55], textual description [2, 13, 31, 3, 36, 47, 60, 46, 1, 27, 7, 51], audio or music [42, 26, 8, 22, 48, 24]. To generate diverse, natural, and high-quality human motions, many generative models have been explored by [2, 27, 36]. Recently, diffusion-based models significantly improved the motion generation performance and diversity [47, 7, 8, 60, 25, 56] with stable training. Specifically, MotionDiffuse [60] represents the first text-based motion diffusion model that provides fine-grained instructions on body parts and achieves arbitrary-length motion synthesis with time-varied text prompts. MDM [47] introduces a motion diffusion model that operates on raw motion data, enabling both high-quality generation and generic conditioning that together comprise a good baseline for new motion generation tasks. The work most relevant to ours is MLD [7], which introduces a motion latent-based diffusion model to enhance generative quality and reduce computational resource requirements. The primary concept involves initially training a VAE [20] for motion embedding, followed by implementing latent diffusion [40] within the learned latent space. However, these diffusion fashions inevitably require considerable sampling steps for motion synthesis during inference, even with some sampling acceleration methods [43]. Thus, we propose MotionLCM, which not only guarantees high-quality motion generation but also enhances efficiency.

2.2 Motion Control

For motion control, MDM [47] and HumanMAC [6] demonstrate zero-shot controlling using diffusion models. Following this, Shafir *et al.* [41] propose PriorMDM to generate long-sequence human motion, enabling joint and trajectory-level control and editing. Additionally, GMD [18] incorporates spatial constraints through a two-stage diffusion approach. However, GMD’s control is limited to 2D pelvis positions, restricting its adaptability across various practical scenarios. OmniControl [54] integrates flexible spatial control signals across different joints by combining analytic spatial guidance and realism guidance into the diffusion model, ensuring that the generated motion closely conforms to the input control signals. TLControl [50] leverages a disentangled latent space for diverse human motion, enabling high-fidelity motion generation aligned with both language descriptions and specified trajectories. However, TLControl requires additional test-time optimization. While these approaches achieve good control quality under given conditions, there remains a significant gap in accelerating the model to real-time performance. We introduce our technical solutions as follows.

3 Method

In this section, we first briefly introduce preliminaries about latent consistency models in Sec. 3.1. Then, we describe how to perform latent consistency distillation for motion generation in Sec. 3.2, followed by our implementation of motion control in latent space in Sec. 3.3.

3.1 Preliminaries

The Consistency Model (CM) [44] introduces a kind of efficient generative model designed for efficient one-step or few-step generation. Given a Probability Flow ODE (*a.k.a.* PF-ODE) that smoothly converts data to noise, the CM is to learn the function $f(\cdot, \cdot)$ (*i.e.*, the solution of the PF-ODE) that maps any points on the ODE trajectory to its origin distribution. The consistency function is formally defined as $f : (\mathbf{x}_t, t) \mapsto \mathbf{x}_\epsilon$, where $t \in [0, T]$, $T > 0$ is a fixed constant, ϵ is a small positive number to avoid numerical instability, and the $\hat{\mathbf{x}}_\epsilon$ can be treated as an approximate sample from the data distribution ($\hat{\mathbf{x}}_\epsilon \sim p_{\text{data}}(\mathbf{x})$). According to [44], the consistency function should satisfy the *self-consistency property* (Definition 1).

Definition 1 Self-consistency Property. The self-consistency property of consistency function $f(\cdot, \cdot)$ can be defined as,

$$f(\mathbf{x}_t, t) = f(\mathbf{x}_{t'}, t'), \forall t, t' \in [\epsilon, T]. \quad (1)$$

As shown in Definition 1, the self-consistency property indicates that for arbitrary pairs of (\mathbf{x}_t, t) on the same PF-ODE trajectory, the outputs of the model should be consistent. The goal of a parameterized consistency model $f_{\Theta}(\cdot, \cdot)$ is to learn a consistency function from data by enforcing the self-consistency property in Eq. (1). To ensure the $f_{\Theta}(\mathbf{x}, \epsilon) = \mathbf{x}$ property, the consistency model is parameterized as follows via skip connections,

$$f_{\Theta}(\mathbf{x}, t) = c_{\text{skip}}(t)\mathbf{x} + c_{\text{out}}(t)\mathbf{F}_{\Theta}(\mathbf{x}, t), \quad (2)$$

where $c_{\text{skip}}(t)$ and $c_{\text{out}}(t)$ are differentiable functions with $c_{\text{skip}}(\epsilon) = 1$ and $c_{\text{out}}(\epsilon) = 0$, and $\mathbf{F}_{\Theta}(\cdot, \cdot)$ is a deep neural network to learn the self-consistency. The CM trained from distilling the knowledge of pre-trained diffusion models is called *Consistency Distillation*. The consistency loss is defined as,

$$\mathcal{L}(\Theta, \Theta^-; \Phi) = \mathbb{E} [d(f_{\Theta}(\mathbf{x}_{t_{n+1}}, t_{n+1}), f_{\Theta^-}(\hat{\mathbf{x}}_{t_n}^{\Phi}, t_n))], \quad (3)$$

where $d(\cdot, \cdot)$ is a chosen metric function for measuring the distance between two samples. $f_{\Theta}(\cdot, \cdot)$ and $f_{\Theta^-}(\cdot, \cdot)$ are referred to as ‘‘online network’’ and ‘‘target network’’ according to [44]. Besides, Θ^- is updated with the exponential moving average (EMA) of the parameter Θ ². In Eq. (3), $\hat{\mathbf{x}}_{t_n}^{\Phi}$ is the one-step estimation from $\mathbf{x}_{t_{n+1}}$. Here, the $\hat{\mathbf{x}}_{t_n}^{\Phi}$ can be formulated as,

$$\hat{\mathbf{x}}_{t_n}^{\Phi} \leftarrow \mathbf{x}_{t_{n+1}} + (t_n - t_{n+1})\Phi(\mathbf{x}_{t_{n+1}}, t_{n+1}), \quad (4)$$

where $\Phi(\cdot, \cdot)$ is a one-step ODE solver applied to PF-ODE.

Latent Consistency Models (LCMs) [32] conduct the consistency distillation in the latent space $D_{\mathbf{z}} = \{(\mathbf{z}, \mathbf{c}) | \mathbf{z} = \mathcal{E}(\mathbf{x}), (\mathbf{x}, \mathbf{c}) \in D\}$, where D denotes the dataset, \mathbf{c} is the given condition, and \mathcal{E} is the pre-trained encoder. Instead of ensuring consistency between adjacent time steps $t_{n+1} \rightarrow t_n$, LCMs [32] are designed to ensure consistency between the current time step and k -step away, *i.e.*, $t_{n+k} \rightarrow t_n$, thereby significantly reducing convergence time costs. As classifier-free guidance (CFG) [16] plays a crucial role in synthesizing high-quality text-aligned visual contents, LCMs integrate CFG into the distillation as follows,

$$\hat{\mathbf{z}}_{t_n}^{\Phi, w} \leftarrow \mathbf{z}_{t_{n+k}} + (1 + w)\Phi(\mathbf{z}_{t_{n+k}}, t_{n+k}, t_n, \mathbf{c}) - w\Phi(\mathbf{z}_{t_{n+k}}, t_{n+k}, t_n, \emptyset). \quad (5)$$

where w denotes the CFG scale which is uniformly sampled from $[w_{\min}, w_{\max}]$ and k is the skipping interval. Besides, the input of Φ is expanded due to the k -step consistency and the given condition.

3.2 MotionLCM: Motion Latent Consistency Model

Motion compression into the latent space. Motivated by [44, 32], we propose MotionLCM (Motion Latent Consistency Model) to tackle the low-efficiency problem in motion diffusion models [47, 60], unleashing the potential of LCM in the motion generation task. Similar to MLD [7], our MotionLCM adopts a consistency model in the motion latent space. We choose the powerful MLD [7] as the underlying diffusion model to distill from. We aim to achieve a few-step (2~4) and even one-step inference without compromising motion quality. In MLD, the autoencoder (\mathcal{E}, \mathcal{D}) is first trained to compress a high dimensional motion into a low dimensional latent vector $\mathbf{z} = \mathcal{E}(\mathbf{x})$, which is then decoded to reconstruct the motion as $\hat{\mathbf{x}} = \mathcal{D}(\mathbf{z})$. Training diffusion models in the motion latent space greatly reduces the computational requirements compared to the vanilla diffusion models trained on raw motion sequences (*i.e.*, motion space) and speeds up the inference process. Accordingly, we take good advantage of the motion latent space for consistency distillation.

Motion latent consistency distillation. An overview of our motion latent consistency distillation is described in Fig. 3 (a). A raw motion sequence $\mathbf{x}_0^{1:N} = \{\mathbf{x}^i\}_{i=1}^N$ is a sequence of human poses represented by $\mathbf{x}^i \in \mathbb{R}^K$, where K is the dimension of the pose representation and N is the number of frames. We follow [13] to use the redundant motion representation for our experiments, which is

²EMA operation: $\Theta^- \leftarrow \text{sg}(\mu\Theta^- + (1 - \mu)\Theta)$, where $\text{sg}(\cdot)$ denotes the stopgrad operation and μ satisfies $0 \leq \mu < 1$.

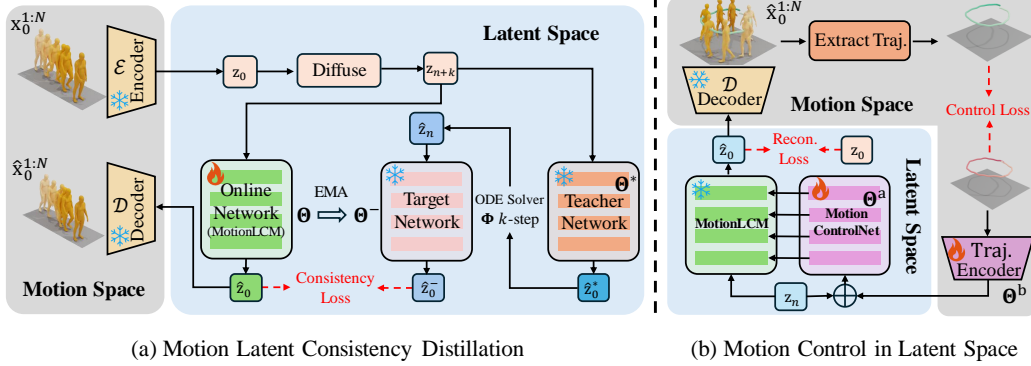


Figure 3: **The overview of MotionLCM.** (a) *Motion Latent Consistency Distillation* (Sec. 3.2). Given a raw motion sequence $\mathbf{x}_0^{1:N}$, a pre-trained VAE encoder first compresses it into the latent space, then performs a forward diffusion to add $n + k$ step noise. Then, the noisy \mathbf{z}_{n+k} is fed into the online network and teacher network to predict the clean latent. The target network takes the k -step estimation results of the teacher output to predict the clean latent. To learn self-consistency, a loss is applied to enforce the output of the online network and target network to be consistent. (b) *Motion Control in Latent Space* (Sec. 3.3). With the powerful MotionLCM trained in the first stage, we incorporate a motion ControlNet into the MotionLCM to achieve controllable motion generation. Furthermore, we leverage the decoded motion to supervise the spatial control signals.

widely used in previous work [47, 60, 7]. As shown in the Fig. 3 (a), given a raw motion sequence $\mathbf{x}_0^{1:N}$, a pre-trained VAE encoder first compresses it into the latent space, $\mathbf{z}_0 = \mathcal{E}(\mathbf{x}_0)$. Then, a forward diffusion operation with $n + k$ steps is conducted to add noise on \mathbf{z}_0 , where k is the skipping interval illustrated in Sec. 3.1. The noisy \mathbf{z}_{n+k} is fed to the frozen teacher network, the trainable online network to predict the clean $\hat{\mathbf{z}}_0^*$, and $\hat{\mathbf{z}}_0$. The target network uses the cleaner $\hat{\mathbf{z}}_n$ obtained by a k -step ODE Solver Φ , such as DDIM [43] to predict the $\hat{\mathbf{z}}_0^-$. Note that $\hat{\mathbf{z}}_0$ and $\hat{\mathbf{z}}_0^-$ are obtained by the consistency function $f(\cdot, \cdot)$ in Eq. (2). Since the classifier-free guidance (CFG) is essential to the condition controlling for diffusion models, we integrate CFG into the latent consistency distillation,

$$\hat{\mathbf{z}}_n \leftarrow \mathbf{z}_{n+k} + (1 + w)\Phi(\mathbf{z}_{n+k}, t_{n+k}, t_n, \mathbf{c}) - w\Phi(\mathbf{z}_{n+k}, t_{n+k}, t_n, \emptyset), \quad (6)$$

where \mathbf{c} is the text condition and w denotes the guidance scale. To ensure the self-consistency property defined in Eq. (1), the consistency distillation loss is designed as,

$$\mathcal{L}_{LCD}(\Theta, \Theta^-) = \mathbb{E}[d(f_{\Theta}(\mathbf{z}_{n+k}, t_{n+k}), f_{\Theta^-}(\hat{\mathbf{z}}_n, t_n))], \quad (7)$$

where $d(\cdot, \cdot)$ is a distance measuring function, such as L2 loss or Huber loss [17]. As discussed in Sec. 3.1, the parameters of the target network are updated with the exponential moving average (EMA) of the parameters of the online network. Here we define the “teacher network” as the pre-trained motion latent diffusion model, *e.g.*, MLD [7]. Accordingly, the online and target networks are initialized with the parameters of the teacher network.

During the inference phase, our MotionLCM can sample high-quality motions in only one step to produce and achieve the fastest runtime (**$\sim 30\text{ms}$ per motion sequence**) compared to other motion diffusion models, which are shown in Fig. 4.

3.3 Controllable Motion Generation in Latent Space

After addressing the low-efficiency issue in the motion latent diffusion model, we delve into another exploration of real-time motion controlling. Inspired by the great success of ControlNet [59] in controllable image generation, we introduce a motion ControlNet on MotionLCM to utilize the trajectory of joint(s) given by users to control the motion generation in MotionLCM. In our MotionLCM, we initialize the motion ControlNet with a trainable copy of MotionLCM. Specifically, each layer in the motion ControlNet is appended with a zero-initialized linear layer for eliminating random noise in the initial training steps.

As shown in Fig. 3 (b), the trajectory is defined as the global absolute positions of the controlling joint(s) following [54]. In our controlling pipeline, we design a Trajectory Encoder consisting of

stacked transformer [49] layers to encode trajectory signals. We append a global token (*i.e.*, [CLS]) before the start of the trajectory sequence as the output vector of the encoder, which is then added to the noisy \mathbf{z}_n and fed into the motion ControlNet. For simplicity, we omit the inputs of text condition \mathbf{c} and time step t (both are fed into the frozen MotionLCM and the trainable motion ControlNet).

Under the guidance of motion ControlNet, MotionLCM predicts the denoised $\hat{\mathbf{z}}_0$. The reconstructed latent can be optimized by the reconstruction loss,

$$\mathcal{L}_{\text{recon}}(\Theta^a, \Theta^b) = \mathbb{E}[d(\hat{\mathbf{z}}_0, \mathbf{z}_0)], \quad (8)$$

where Θ^a and Θ^b are the parameters of the motion ControlNet and Trajectory Encoder. However, during training, the sole reconstruction supervision in the latent space is insufficient, which is also verified in our motion control experiments in Tab. 5. We argue this is because the controllable motion generation requires more detailed constraints, which cannot be effectively provided solely by the reconstruction loss in the latent space. Unlike previous methods like OmniControl [54], which directly diffuse in motion space, allowing explicit supervision of control signals, effectively supervising control signals in the latent space is non-trivial. Therefore, we utilize the frozen VAE [20] decoder $\mathcal{D}(\cdot)$ to decode $\hat{\mathbf{z}}_0$ into the motion space, obtaining the predicted motion $\hat{\mathbf{x}}_0$, thereby introducing the controlling loss as follows,

$$\mathcal{L}_{\text{control}}(\Theta^a, \Theta^b) = \mathbb{E}\left[\frac{\sum_i \sum_j m_{ij} \|R(\hat{\mathbf{x}}_0)_{ij} - R(\mathbf{x}_0)_{ij}\|_2^2}{\sum_i \sum_j m_{ij}}\right], \quad (9)$$

where $R(\cdot)$ converts the joint’s local positions to global absolute locations, $m_{ij} \in \{0, 1\}$ is the binary joint mask at frame i for the joint j . Then we optimize the parameters in motion ControlNet Θ^a and Trajectory Encoder Θ^b with an overall objective,

$$\Theta^a, \Theta^b = \underset{\Theta^a, \Theta^b}{\text{argmin}}(\mathcal{L}_{\text{recon}} + \lambda \mathcal{L}_{\text{control}}), \quad (10)$$

where λ is the weight to balance the two losses. This design enables explicit control signals to directly influence the generation process, similar to controlling other latent-free diffusion models for motion generation [18]. Comprehensive experiments demonstrate that introduced supervision is very helpful in improving the quality of control, which will be introduced in the following section.

4 Experiments

In this section, we first present the experimental setup details in Sec. 4.1. Subsequently, we provide quantitative and qualitative comparisons to evaluate the effectiveness of our proposed MotionLCM framework in Sec. 4.2 and Sec. 4.3. Finally, we conduct comprehensive ablation studies on MotionLCM in Sec. 4.4. These experiments demonstrate the effectiveness of the proposed method.

4.1 Experimental setup

Datasets. Our experiments are conducted on the popular HumanML3D [13] dataset which offers an extensive collection of human motions, featuring 14,616 unique human motion sequences from AMASS [33] and HumanAct12 [15], paired with 44,970 textual descriptions. For a fair comparison with previous methods [13], we take the redundant motion representation, including root velocity, root height, local joint positions, velocities, rotations in root space, and the foot contact binary labels.

Evaluation metrics. We extend the evaluation metrics of previous works [13, 54, 7]. **(1) Time costs:** we report the Average Inference Time per Sentence (AITS) [7] to evaluate the inference efficiency of models. **(2) Motion quality:** Frechet Inception Distance (FID) is adopted as a principal metric to evaluate the feature distributions between the generated and real motions. The feature extractor employed is from [13]. **(3) Motion diversity:** MultiModality (MModality) measures the generation diversity conditioned on the same text and Diversity calculates variance through features [13]. **(4) Condition matching:** Following [13], we calculate the motion-retrieval precision (R-Precision) to report the text-motion Top 1/2/3 matching accuracy and Multimodal Distance (MM Dist) calculates the distance between motions and texts. **(5) Control error:** Trajectory error (Traj. err.) quantifies the proportions of unsuccessful trajectories, characterized by any joint location error surpassing a predetermined threshold. Location error (Loc. err.) represents the proportion of joint locations that

Methods	AITS ↓	R-Precision ↑			FID ↓	MM Dist ↓	Diversity →	MModality ↑
		Top 1	Top 2	Top 3				
Real	-	0.511±.003	0.703±.003	0.797±.002	0.002±.000	2.794±.008	9.503±.065	-
Seq2Seq [38]	-	0.180±.002	0.300±.002	0.396±.002	11.75±.035	5.529±.007	6.223±.061	-
LJ2P [2]	-	0.246±.001	0.387±.002	0.486±.002	11.02±.046	5.296±.008	7.676±.058	-
T2G [4]	-	0.165±.001	0.267±.002	0.345±.002	7.664±.030	6.030±.008	6.409±.071	-
Hier [11]	-	0.301±.002	0.425±.002	0.552±.004	6.532±.024	5.012±.018	8.332±.042	-
TEMOS [36]	0.017	0.424±.002	0.612±.002	0.722±.002	3.734±.028	3.703±.008	8.973±.071	0.368±.018
T2M [13]	0.038	0.457±.002	0.639±.003	0.740±.003	1.067±.002	3.340±.008	9.188±.002	2.090±.083
MDM [47]	24.74	0.320±.005	0.498±.004	0.611±.007	0.544±.044	5.566±.027	9.559 ±.086	2.799 ±.072
MotionDiffuse [60]	14.74	0.491±.001	0.681±.0.001	0.782±.001	0.630±.001	3.113±.001	<u>9.410</u> ±.049	1.553±.042
MLD [7]	0.217	0.481±.003	0.673±.003	0.772±.002	0.473±.013	3.196±.010	9.724±.082	<u>2.413</u> ±.079
MLD* [7]	0.225	<u>0.504</u> ±.002	0.698±.003	0.796±.002	0.450±.011	3.052±.009	9.634±.064	2.267±.082
MotionLCM (1-Step)	0.030	0.502±.003	<u>0.701</u> ±.002	<u>0.803</u> ±.002	0.467±.012	3.022±.009	9.631±.066	2.172±.082
MotionLCM (2-Step)	<u>0.035</u>	0.505 ±.003	0.705 ±.002	0.805 ±.002	<u>0.368</u> ±.011	2.986 ±.008	9.640±.052	2.187±.094
MotionLCM (4-Step)	0.043	0.502±.003	0.698±.002	0.798±.002	0.304 ±.012	<u>3.012</u> ±.007	9.607±.066	2.259±.092

Table 1: Comparison of text-conditional motion synthesis on HumanML3D [13] dataset. We compute suggested metrics following [13]. We repeat the evaluation 20 times for each metric and report the average with a 95% confidence interval. “→” indicates that the closer to the real data, the better. **Bold** and underline indicate the best and the second best result. “*” denotes the reproduced version of MLD [7]. The performance of our MotionLCM in **one-step inference (30ms)** surpasses all state-of-the-art models, providing ample evidence for the effectiveness of latent consistency distillation.

are not reached within a specified threshold distance. Average error (Avg. err.) denotes the mean distance between the joint positions in the generated motion and the given control trajectories.

Implementation details. Our baseline motion diffusion model is based on MLD [7]. We reproduce MLD with higher performance. Unless otherwise specified, all our experiments are conducted on this model. For MotionLCM, we employ an AdamW [19] optimizer for 96K iterations using a cosine decay learning rate scheduler and 1K iterations of linear warm-up. A batch size of 256 and a learning rate of 2e-4 are used. We set the training guidance scale range $[w_{\min}, w_{\max}] = [5, 15]$ with the testing guidance scale as 7.5, and adopt the EMA rate $\mu = 0.95$ by default. We use DDIM-Solver [43] with skipping step $k = 20$ and choose the Huber [17] loss as the distance measuring function d . For motion ControlNet, we employ an AdamW [19] for optimizer for longer training of 192K iterations with 1K iterations of linear warm-up. The batch size and learning rate are set as 128 and 1e-4. The learning rate scheduler is the same as the first stage. We follow [54] to use the global absolute locations of the control joint to train motion ControlNet. For the training objective, we employ d as the L2 loss and set the control loss weight λ to 1.0 by default. We implement our model using PyTorch [34] with training on one NVIDIA RTX 4090 GPU. We use one Tesla V100 GPU to align the text-to-motion inference experiment settings in MLD [7]. For controllable motion generation, all models are evaluated for their inference speed on one NVIDIA RTX 4090 GPU.

4.2 Comparisons on Text-to-motion

In the following part, we first evaluate our MotionLCM on the text-to-motion (T2M) task. We compare our method with some T2M baselines on HumanML3D [13] with suggested metrics [13] under the 95% confidence interval from 20 times running. As MotionLCM is based on MLD, we mainly focus on the performance compared with MLD. For evaluating time efficiency, we compare the Average Inference Time per Sentence (AITS) with TEMOS [36], T2M [13], MDM [47], MotionDiffuse [60] and MLD [7]. The results are borrowed from MLD [7]. The deterministic methods [38, 2, 11, 4], are unable to produce diverse results from a single input and thus we leave their MModality metrics empty. For the quantitative results, as shown in Tab. 1, our MotionLCM boasts an impressive real-time runtime efficiency, averaging around **30ms per motion sequence** during inference. This performance exceeds that of previous diffusion-based methods [47, 60, 7] and even surpasses MLD [7] by an order of magnitude. Furthermore, despite employing only one-step inference, our MotionLCM can approximate or even surpass the performance of MLD [7] (DDIM [43] 50 steps). With two-step inference, we achieve the best R-Precision and MM Dist metrics, while increasing the sampling steps to four yields the best FID. The above results demonstrate the effectiveness of latent consistency

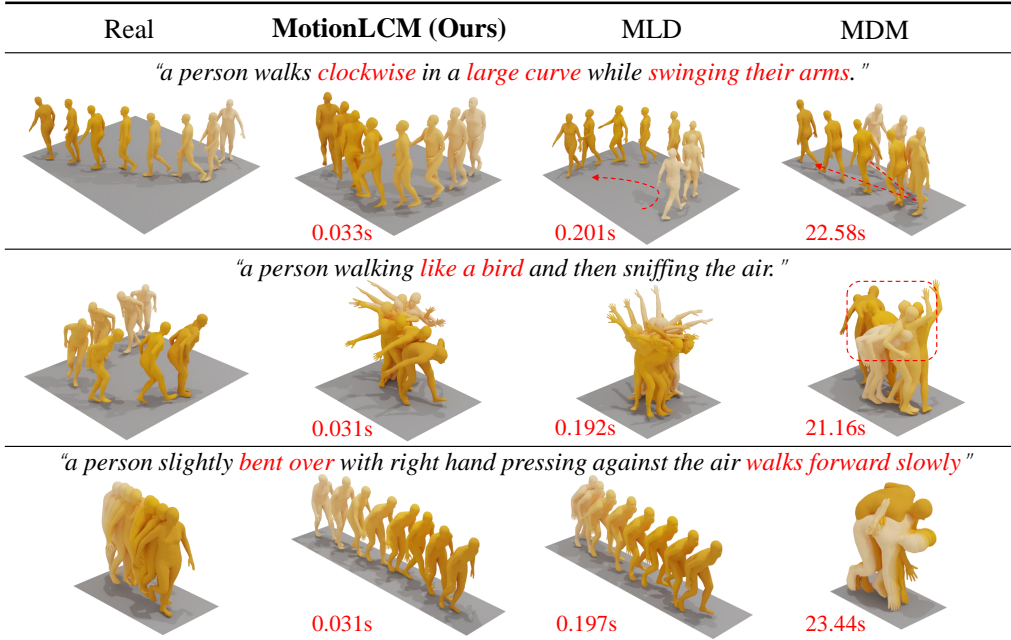


Figure 4: Qualitative comparison of the state-of-the-art methods in text-to-motion task. We provide the visualized motion results and real references from three text prompts. With only one-step inference, MotionLCM achieves the fastest motion generation while producing high-quality movements that closely match the textual descriptions.

Methods	AITs ↓	FID ↓	R-Precision ↑ Top 3	Diversity →	Traj. err. ↓ (50cm)	Loc. err. ↓ (50cm)	Avg. err. ↓
Real	-	0.002	0.797	9.503	0.000	0.000	0.000
MDM [47]	18.84	0.698	0.602	9.197	0.4022	0.3076	0.5959
PriorMDM [47]	18.84	0.475	0.583	9.156	0.3457	0.2132	0.4417
GMD* [18]	126.10	0.576	0.665	9.206	0.0931	0.0321	0.1439
OmniControl* [54]	72.88	0.218	0.687	9.422	0.0387	0.0096	0.0338
OmniControl [54]	37.80	0.212	0.678	9.773	0.3041	0.1873	0.3226
MotionLCM	0.034 (↑550×)	0.531	0.752	9.253	0.1887	0.0769	0.1897

Table 2: Quantitative results of comparison with state-of-the-art methods on HumanML3D [13] test set. “→” means closer to real data is better. “*” means the model using guided diffusion [9]. All models are trained on pelvis control.

distillation. For the qualitative results, as shown in Fig. 4, MotionLCM not only accelerates motion generation to real-time speeds but also delivers high-quality outputs, aligning with textual descriptions.

4.3 Comparisons on Controllable Motion Generation

As shown in Tab. 2, we compare our MotionLCM with [41, 18, 54] and report metrics from [54, 7]. Due to GMD [18] and OmniControl [18] utilizing high-cost guided-diffusion [9], we reimplement OmniControl without using guided diffusion for a fair comparison. The results indicate that MotionLCM performs well in motion control and achieves state-of-the-art performance in text-motion alignment, as demonstrated by R-Precision. Even without guided diffusion, inference for a single motion in OmniControl [54] still takes around 37 seconds, which is unacceptable for real-time applications. In contrast, MotionLCM only requires ~0.03 seconds, achieving a speedup of nearly ↑1100× over OmniControl and ↑550× over the PriorMDM (the fastest method).

Methods	R-Precision \uparrow Top 1	FID \downarrow	MM Dist \downarrow	Diversity \rightarrow	MModality \uparrow
Real	0.511 \pm .003	0.002 \pm .000	2.794 \pm .008	9.503 \pm .065	-
MotionLCM ($w \in [5, 15]$)	0.502 \pm .003	0.467 \pm .012	3.022 \pm .009	9.631 \pm .066	2.172 \pm .082
MotionLCM ($w \in [2, 18]$)	0.497 \pm .003	0.481 \pm .009	3.030 \pm .010	9.644 \pm .073	2.226 \pm .091
MotionLCM ($w = 7.5$)	0.486 \pm .002	0.479 \pm .009	3.094 \pm .009	9.610 \pm .072	2.320 \pm .097
MotionLCM ($\mu = 0.95$)	0.502 \pm .003	0.467 \pm .012	3.022 \pm .009	9.631 \pm .066	2.172 \pm .082
MotionLCM ($\mu = 0.50$)	0.498 \pm .003	0.478 \pm .009	3.022 \pm .010	9.655 \pm .071	2.188 \pm .087
MotionLCM ($\mu = 0$)	0.499 \pm .003	0.505 \pm .008	3.018 \pm .009	9.706 \pm .070	2.123 \pm .085
MotionLCM ($k = 50$)	0.488 \pm .003	0.547 \pm .011	3.096 \pm .010	9.511 \pm .074	2.324 \pm .091
MotionLCM ($k = 20$)	0.502 \pm .003	0.467 \pm .012	3.022 \pm .009	9.631 \pm .066	2.172 \pm .082
MotionLCM ($k = 10$)	0.497 \pm .003	0.449 \pm .009	3.017 \pm .010	9.693 \pm .075	2.133 \pm .086
MotionLCM ($k = 5$)	0.488 \pm .003	0.438 \pm .009	3.044 \pm .009	9.647 \pm .074	2.147 \pm .083
MotionLCM ($k = 1$)	0.442 \pm .002	0.635 \pm .011	3.255 \pm .008	9.384 \pm .080	2.146 \pm .075
MotionLCM (w/ Huber)	0.502 \pm .003	0.467 \pm .012	3.022 \pm .009	9.631 \pm .066	2.172 \pm .082
MotionLCM (w/ L2)	0.486 \pm .002	0.622 \pm .010	3.114 \pm .009	9.573 \pm .069	2.218 \pm .086

Table 3: Ablation study on different training guidance scale range $[w_{\min}, w_{\max}]$, EMA rate μ , skipping interval k and loss type. We use metrics in Tab. 1 and adopt a one-step inference setting with the testing CFG scale of 7.5 for fair comparison.

Methods	R-Precision (Top 3) \uparrow			FID \downarrow		
	1-Step	2-Step	4-Step	1-Step	2-Step	4-Step
DDIM [43]	0.337 \pm .002	0.375 \pm .002	0.460 \pm .003	4.022 \pm .043	2.802 \pm .038	0.966 \pm .018
DPM [29]	0.337 \pm .002	0.374 \pm .002	0.477 \pm .002	4.022 \pm .043	2.798 \pm .038	0.727 \pm .015
DPM++ [30]	0.337 \pm .002	0.375 \pm .002	0.478 \pm .003	4.022 \pm .043	2.798 \pm .038	0.684 \pm .015
MotionLCM	0.803 \pm .002	0.805 \pm .002	0.798 \pm .002	0.467 \pm .012	0.368 \pm .011	0.304 \pm .012

Table 4: Quantitative results with the testing CFG scale $w = 7.5$. MotionLCM notably outperforms baseline methods on HumanML3D [13] dataset, demonstrating the effectiveness of latent consistency distillation. **Bold** indicates the best result.

4.4 Ablation Studies

Impact of the hyperparameters of training MotionLCM. We conduct a comprehensive analysis of the training hyperparameters of MotionLCM, including the training guidance scale range $[w_{\min}, w_{\max}]$, EMA rate μ , skipping interval k , and the loss type. We summarize the evaluation results based on one-step inference in Tab. 3. We find out that using a dynamic training guidance scale during training leads to an improvement in model performance compared to using a static training guidance scale, such as $w = 7.5$. Additionally, an excessively large range for the training guidance scale can also negatively impact the performance of the model (*e.g.*, $w \in [2, 18]$). Regarding the EMA rate μ , we observe that the larger the value of μ , the better the performance of the model, which indicates that maintaining a slower update rate for the target network Θ^- helps improve the performance of latent consistency distillation. When the skipping interval k continues to increase, the performance of the distillation model improves continuously, but larger values of k (*e.g.*, $k = 50$) may result in inferior results. As for the loss type, the Huber loss [17] significantly outperforms the L2 loss, demonstrating the superior robustness of the method.

Comparison to other ODE Solvers. To validate the effectiveness of latent consistency distillation, we compare three ODE solvers (DDIM [43], DPM [29], DPM++ [30]). The quantitative results in Tab. 4 demonstrate that our MotionLCM notably outperforms baseline methods. Moreover, unlike DDIM [43], DPM [29], and DPM++ [30], requiring more peak memory per sampling step when using CFG, MotionLCM only requires one forward pass, saving both time and memory costs.

Methods	AITs	FID ↓	R-Precision ↑ Top 3	Diversity →	Traj. err. ↓ (50cm)	Loc. err. ↓ (50cm)	Avg. err. ↓
Real	-	0.002	0.797	9.503	0.000	0.000	0.000
MLD [7] ($\lambda = 0$)	0.447	0.784	0.722	9.371	0.3666	0.2150	0.3937
MLD [7] ($\lambda = 1$)	0.447	0.829	0.744	9.221	0.3139	0.1710	0.2893
MotionLCM ($\lambda = 0$)	0.034	0.325	0.763	9.164	0.2693	0.1354	0.2805
MoitonLCM ($\lambda = 1$)	0.034	0.531	0.752	9.253	0.1887	0.0769	0.1897

Table 5: Quantitative experimental results of motion control for MLD [7] and MotionLCM. The latent generated by MotionLCM is more beneficial for training motion ControlNet compared to MLD [7]. The two models are trained on pelvis control.

The effectiveness of MotioLCM latent for motion control. To verify the effectiveness of the latent generated by our MotionLCM compared to MLD for training motion ControlNet, we conducted the following two sets of experiments: one with $\lambda = 0$, meaning supervision only in the latent space, and the other with $\lambda = 1$, indicating additional supervision in the motion space with a control loss weight of 1. We present the experimental results in Tab. 5. It can be observed that under the same experimental settings, MotionLCM maintains higher fidelity and significantly outperforms MLD in motion control performance. Furthermore, in terms of inference speed, MLD utilizes DDIM [43] with 50 steps, while MotionLCM only requires one-step inference, resulting in a $\sim\uparrow 13\times$ speedup. This demonstrates the effectiveness of the latent generated by MotionLCM for training motion ControlNet.

5 Conclusion and Limitation

Conclusion. This work proposes an efficient controllable motion generation framework, MotionLCM. Following the core pipeline of the previous controllable motion generation framework, MotionLCM is based on a motion latent diffusion model. By introducing latent consistency distillation, MotionLM enjoys the trade-off between runtime efficiency and generation quality. Moreover, thanks to the motion ControlNet manipulation in the latent space, our method enjoys good controlling ability with given conditions. Extensive experiments show the effectiveness of our method and key designs.

Limitation and future work. Although MotionLCM enjoys a good trade-off between generation quality and efficiency in the text-to-motion task. However, for the motion control task, OmniControl [54] and GMD [18], which utilize guided diffusion [9], still outperform MotionLCM significantly in terms of performance. Besides, we do not resolve the physical implausible problem of generated motion and learn motion distribution from noisy or anomalous data [5, 52]. We leave these issues as our future work. Except for these, we will also focus on automatically annotating high-quality texts for motions, targeting building a closed-loop of bi-directional text-motion synthesis, which is quite essential to a larger data scale.

Acknowledgement

The author team would like to acknowledge Shunlin Lu (The Chinese University of Hong Kong, Shenzhen), Yiming Xie (Northeastern University), Zhiyang Dou (The University of Hong Kong), and Jiahao Cui (Sun Yat-sen University) for their helpful technical discussion and suggestions.

References

- [1] Ahn, H., Ha, T., Choi, Y., Yoo, H., Oh, S.: Text2action: Generative adversarial synthesis from language to action. In: ICRA. pp. 5915–5920 (2018)
- [2] Ahuja, C., Morency, L.P.: Language2pose: Natural language grounded pose forecasting. In: 3DV. pp. 719–728 (2019)
- [3] Athanasiou, N., Petrovich, M., Black, M.J., Varol, G.: Teach: Temporal action composition for 3d humans. In: 3DV. pp. 414–423 (2022)
- [4] Bhattacharya, U., Rewkowski, N., Banerjee, A., Guhan, P., Bera, A., Manocha, D.: Text2gestures: A transformer-based network for generating emotive body gestures for virtual agents. In: VR. pp. 1–10 (2021)
- [5] Chen, L.H., Li, H., Zhang, W., Huang, J., Ma, X., Cui, J., Li, N., Yoo, J.: Anomman: Detect anomalies on multi-view attributed networks. *Information Sciences* **628**, 1–21 (2023)
- [6] Chen, L.H., Zhang, J., Li, Y., Pang, Y., Xia, X., Liu, T.: Humanmac: Masked motion completion for human motion prediction. In: ICCV. pp. 9544–9555 (2023)
- [7] Chen, X., Jiang, B., Liu, W., Huang, Z., Fu, B., Chen, T., Yu, G.: Executing your commands via motion diffusion in latent space. In: CVPR. pp. 18000–18010 (2023)
- [8] Dabral, R., Mughal, M.H., Golyanik, V., Theobalt, C.: Mofusion: A framework for denoising-diffusion-based motion synthesis. In: CVPR. pp. 9760–9770 (2023)
- [9] Dhariwal, P., Nichol, A.: Diffusion models beat gans on image synthesis. *NeurIPS* pp. 8780–8794 (2021)
- [10] Dou, Z., Chen, X., Fan, Q., Komura, T., Wang, W.: C-ase: Learning conditional adversarial skill embeddings for physics-based characters. In: SIGGRAPH Asia. pp. 1–11 (2023)
- [11] Ghosh, A., Cheema, N., Oguz, C., Theobalt, C., Slusallek, P.: Synthesis of compositional animations from textual descriptions. In: ICCV. pp. 1396–1406 (2021)
- [12] Guo, C., Mu, Y., Javed, M.G., Wang, S., Cheng, L.: Momask: Generative masked modeling of 3d human motions. In: CVPR (2024)
- [13] Guo, C., Zou, S., Zuo, X., Wang, S., Ji, W., Li, X., Cheng, L.: Generating diverse and natural 3d human motions from text. In: CVPR. pp. 5152–5161 (2022)
- [14] Guo, C., Zuo, X., Wang, S., Cheng, L.: Tm2t: Stochastic and tokenized modeling for the reciprocal generation of 3d human motions and texts. In: ECCV. pp. 580–597 (2022)
- [15] Guo, C., Zuo, X., Wang, S., Zou, S., Sun, Q., Deng, A., Gong, M., Cheng, L.: Action2motion: Conditioned generation of 3d human motions. In: ACM MM. pp. 2021–2029 (2020)
- [16] Ho, J., Salimans, T.: Classifier-free diffusion guidance. *arXiv preprint arXiv:2207.12598* (2022)
- [17] Huber, P.J.: Robust estimation of a location parameter. *The Annals of Mathematical Statistics* **35**(1), 73 – 101 (1964)
- [18] Karunratanakul, K., Preechakul, K., Suwajanakorn, S., Tang, S.: Guided motion diffusion for controllable human motion synthesis. In: ICCV. pp. 2151–2162 (2023)
- [19] Kingma, D.P., Ba, J.: Adam: A method for stochastic optimization. *arXiv preprint arXiv:1412.6980* (2014)
- [20] Kingma, D.P., Welling, M.: Auto-encoding variational bayes. *arXiv preprint arXiv:1312.6114* (2013)
- [21] Lee, T., Moon, G., Lee, K.M.: Multiact: Long-term 3d human motion generation from multiple action labels. In: AAAI. pp. 1231–1239 (2023)
- [22] Li, B., Zhao, Y., Zhelun, S., Sheng, L.: Danceformer: Music conditioned 3d dance generation with parametric motion transformer. In: AAAI. pp. 1272–1279 (2022)
- [23] Li, P., Aberman, K., Zhang, Z., Hanocka, R., Sorkine-Hornung, O.: Ganimator: Neural motion synthesis from a single sequence. *TOG* **41**(4), 1–12 (2022)
- [24] Li, R., Zhang, Y., Zhang, Y., Zhang, H., Guo, J., Zhang, Y., Liu, Y., Li, X.: Lodge: A coarse to fine diffusion network for long dance generation guided by the characteristic dance primitives. In: CVPR (2024)

- [25] Li, R., Zhao, J., Zhang, Y., Su, M., Ren, Z., Zhang, H., Tang, Y., Li, X.: Finedance: A fine-grained choreography dataset for 3d full body dance generation. In: ICCV. pp. 10234–10243 (2023)
- [26] Li, R., Yang, S., Ross, D.A., Kanazawa, A.: Ai choreographer: Music conditioned 3d dance generation with aist++. In: ICCV. pp. 13401–13412 (2021)
- [27] Lin, X., Amer, M.R.: Human motion modeling using dvgans. arXiv preprint arXiv:1804.10652 (2018)
- [28] Liu, J., Dai, W., Wang, C., Cheng, Y., Tang, Y., Tong, X.: Plan, posture and go: Towards open-world text-to-motion generation. arXiv preprint arXiv:2312.14828 (2023)
- [29] Lu, C., Zhou, Y., Bao, F., Chen, J., Li, C., Zhu, J.: Dpm-solver: A fast ode solver for diffusion probabilistic model sampling in around 10 steps. NeurIPS pp. 5775–5787 (2022)
- [30] Lu, C., Zhou, Y., Bao, F., Chen, J., Li, C., Zhu, J.: Dpm-solver++: Fast solver for guided sampling of diffusion probabilistic models. arXiv preprint arXiv:2211.01095 (2022)
- [31] Lu, S., Chen, L.H., Zeng, A., Lin, J., Zhang, R., Zhang, L., Shum, H.Y.: Humantomato: Text-aligned whole-body motion generation. arXiv preprint arXiv:2310.12978 (2023)
- [32] Luo, S., Tan, Y., Huang, L., Li, J., Zhao, H.: Latent consistency models: Synthesizing high-resolution images with few-step inference. arXiv preprint arXiv:2310.04378 (2023)
- [33] Mahmood, N., Ghorbani, N., Troje, N.F., Pons-Moll, G., Black, M.J.: Amass: Archive of motion capture as surface shapes. In: ICCV. pp. 5442–5451 (2019)
- [34] Paszke, A., Gross, S., Massa, F., Lerer, A., Bradbury, J., Chanan, G., Killeen, T., Lin, Z., Gimelshein, N., Antiga, L., et al.: Pytorch: An imperative style, high-performance deep learning library. NeurIPS **32** (2019)
- [35] Petrovich, M., Black, M.J., Varol, G.: Action-conditioned 3d human motion synthesis with transformer vae. In: ICCV. pp. 10985–10995 (2021)
- [36] Petrovich, M., Black, M.J., Varol, G.: Temos: Generating diverse human motions from textual descriptions. In: ECCV. pp. 480–497 (2022)
- [37] Plappert, M., Mandery, C., Asfour, T.: The kit motion-language dataset. Big data **4**(4), 236–252 (2016)
- [38] Plappert, M., Mandery, C., Asfour, T.: Learning a bidirectional mapping between human whole-body motion and natural language using deep recurrent neural networks. Robotics and Autonomous Systems **109**, 13–26 (2018)
- [39] Raab, S., Leibovitch, I., Li, P., Aberman, K., Sorkine-Hornung, O., Cohen-Or, D.: Modi: Unconditional motion synthesis from diverse data. In: CVPR. pp. 13873–13883 (2023)
- [40] Rombach, R., Blattmann, A., Lorenz, D., Esser, P., Ommer, B.: High-resolution image synthesis with latent diffusion models. In: CVPR. pp. 10684–10695 (2022)
- [41] Shafir, Y., Tevet, G., Kapon, R., Bermano, A.H.: Human motion diffusion as a generative prior. In: ICLR (2023)
- [42] Siyao, L., Yu, W., Gu, T., Lin, C., Wang, Q., Qian, C., Loy, C.C., Liu, Z.: Bailando: 3d dance generation by actor-critic gpt with choreographic memory. In: Proceedings of the IEEE/CVF Conference on Computer Vision and Pattern Recognition. pp. 11050–11059 (2022)
- [43] Song, J., Meng, C., Ermon, S.: Denoising diffusion implicit models. In: ICLR (2021)
- [44] Song, Y., Dhariwal, P., Chen, M., Sutskever, I.: Consistency models. In: ICML (2023)
- [45] Tang, Y., Liu, J., Liu, A., Yang, B., Dai, W., Rao, Y., Lu, J., Zhou, J., Li, X.: Flag3d: A 3d fitness activity dataset with language instruction. In: CVPR. pp. 22106–22117 (2023)
- [46] Tevet, G., Gordon, B., Hertz, A., Bermano, A.H., Cohen-Or, D.: Motionclip: Exposing human motion generation to clip space. In: ECCV. pp. 358–374 (2022)
- [47] Tevet, G., Raab, S., Gordon, B., Shafir, Y., Cohen-Or, D., Bermano, A.H.: Human motion diffusion model. In: ICLR (2022)
- [48] Tseng, J., Castellon, R., Liu, K.: Edge: Editable dance generation from music. In: CVPR. pp. 448–458 (2023)

- [49] Vaswani, A., Shazeer, N., Parmar, N., Uszkoreit, J., Jones, L., Gomez, A.N., Kaiser, Ł., Polosukhin, I.: Attention is all you need. *NeurIPS* (2017)
- [50] Wan, W., Dou, Z., Komura, T., Wang, W., Jayaraman, D., Liu, L.: Tlcontrol: Trajectory and language control for human motion synthesis. *arXiv preprint arXiv:2311.17135* (2023)
- [51] Wang, Z., Chen, Y., Liu, T., Zhu, Y., Liang, W., Huang, S.: Humanise: Language-conditioned human motion generation in 3d scenes. *NeurIPS* pp. 14959–14971 (2022)
- [52] Xia, X., Liu, T., Wang, N., Han, B., Gong, C., Niu, G., Sugiyama, M.: Are anchor points really indispensable in label-noise learning? *NeurIPS* **32** (2019)
- [53] Xiao, Z., Wang, T., Wang, J., Cao, J., Zhang, W., Dai, B., Lin, D., Pang, J.: Unified human-scene interaction via prompted chain-of-contacts. In: *ICLR* (2024)
- [54] Xie, Y., Jampani, V., Zhong, L., Sun, D., Jiang, H.: Omnicontrol: Control any joint at any time for human motion generation. In: *ICLR* (2023)
- [55] Xu, L., Song, Z., Wang, D., Su, J., Fang, Z., Ding, C., Gan, W., Yan, Y., Jin, X., Yang, X., et al.: Actformer: A gan-based transformer towards general action-conditioned 3d human motion generation. In: *ICCV*. pp. 2228–2238 (2023)
- [56] Xu, S., Li, Z., Wang, Y.X., Gui, L.Y.: Interdiff: Generating 3d human-object interactions with physics-informed diffusion. In: *ICCV*. pp. 14928–14940 (2023)
- [57] Yan, S., Li, Z., Xiong, Y., Yan, H., Lin, D.: Convolutional sequence generation for skeleton-based action synthesis. In: *ICCV*. pp. 4394–4402 (2019)
- [58] Yuan, Y., Song, J., Iqbal, U., Vahdat, A., Kautz, J.: Physdiff: Physics-guided human motion diffusion model. In: *ICCV* (2023)
- [59] Zhang, L., Rao, A., Agrawala, M.: Adding conditional control to text-to-image diffusion models. In: *ICCV*. pp. 3836–3847 (2023)
- [60] Zhang, M., Cai, Z., Pan, L., Hong, F., Guo, X., Yang, L., Liu, Z.: Motiondiffuse: Text-driven human motion generation with diffusion model. *arXiv preprint arXiv:2208.15001* (2022)
- [61] Zhang, M., Guo, X., Pan, L., Cai, Z., Hong, F., Li, H., Yang, L., Liu, Z.: Remodiffuse: Retrieval-augmented motion diffusion model. In: *ICCV* (2023)
- [62] Zhang, Y., Black, M.J., Tang, S.: Perpetual motion: Generating unbounded human motion. *arXiv preprint arXiv:2007.13886* (2020)
- [63] Zhao, R., Su, H., Ji, Q.: Bayesian adversarial human motion synthesis. In: *CVPR*. pp. 6225–6234 (2020)

Appendix for MotionLCM

In the appendix, we provide additional details and experiments not included in the main text.

- Appendix A: Additional experiments.
- Appendix B: Details of the evaluation metrics.
- Appendix C: Supplementary quantitative results.

A Additional Experiments

A.1 Impact of the control loss weight λ .

As shown in Tab. 6, we conduct ablation studies on the control loss weight λ . We found that as the weight increases, the quality of motion generated continuously decreases (as indicated by FID), despite improving motion control performance. To balance motion quality and motion control performance, we choose $\lambda = 1$ to report our final results.

Methods	FID ↓	R-Precision ↑ Top 3	Diversity →	Traj. err. ↓ (50cm)	Loc. err. ↓ (50cm)	Avg. err. ↓
Real	0.002	0.797	9.503	0.000	0.000	0.000
MotionLCM ($\lambda = 0.0$)	0.325	0.763	9.164	0.2693	0.1354	0.2805
MotionLCM ($\lambda = 0.1$)	0.370	0.771	9.096	0.2318	0.1113	0.2367
MotionLCM ($\lambda = 1.0$)	0.531	0.752	9.253	0.1887	0.0769	0.1897
MotionLCM ($\lambda = 2.0$)	0.807	0.748	8.926	0.1482	0.0579	0.1741
MotionLCM ($\lambda = 5.0$)	1.724	0.725	8.902	0.1541	0.0468	0.1594

Table 6: Ablation studies on the control loss weight λ . We report the results on pelvis control. Increasing the control loss weight can enhance motion control performance but would decrease the motion quality. Thus, we use $\lambda = 1$ to balance the two aspects.

B Metric Definitions

Time costs: To assess the inference efficiency of models, we follow [7] to report the Average Inference Time per Sentence (AITS) measured in seconds. We calculate AITS on the test set of HumanML3D [13], set the batch size to 1, and exclude the time cost for model and dataset loading.

Motion quality: Fréchet Inception Distance (FID) measures the distributional difference between the generated and real motions, calculated using the feature extractor associated with a specific dataset.

Motion diversity: Following [15, 14], we report Diversity and MultiModality to evaluate the generated motion diversity. Diversity measures the variance of the generated motions across the whole set. Specifically, two subsets of the same size S_d are randomly sampled from all generated motions with their extracted motion feature vectors $\{\mathbf{v}_1, \dots, \mathbf{v}_{S_d}\}$ and $\{\mathbf{v}'_1, \dots, \mathbf{v}'_{S_d}\}$. The diversity metric is defined as follows,

$$\text{Diversity} = \frac{1}{S_d} \sum_{i=1}^{S_d} \|\mathbf{v}_i - \mathbf{v}'_i\|_2. \quad (11)$$

Different from Diversity, MultiModality (MModality) measures how much the generated motions diversify within each text description. Specifically, a set of text descriptions with size C is randomly sampled from all descriptions. Then we randomly sample two subsets with the same size I from all generated motions conditioned by c -th text description, with extracted feature vectors $\{\mathbf{v}_{c,1}, \dots, \mathbf{v}_{c,I}\}$ and $\{\mathbf{v}'_{c,1}, \dots, \mathbf{v}'_{c,I}\}$. MModality is formalized as follows,

$$\text{MModality} = \frac{1}{C \times I} \sum_{c=1}^C \sum_{i=1}^I \|\mathbf{v}_{c,i} - \mathbf{v}'_{c,i}\|_2. \quad (12)$$

Condition matching: [13] provides motion/text feature extractors to generate geometrically closed features for matched text-motion pairs and vice versa. Under this feature space, evaluating motion-retrieval precision (R-Precision) involves mixing the generated motion with 31 mismatched motions and then calculating the text-motion Top-1/2/3 matching accuracy. Multimodal Distance (MM Dist) calculates the distance between the generated motion and text.

Control error: Following [54], we report Trajectory, Location, and Average errors to assess the motion control performance. Trajectory error (Traj. err.) is defined as the proportions of unsuccessful trajectories, *i.e.*, if there is a joint in the generated motion that exceeds a certain distance threshold from the corresponding joint in the given control trajectory, it is viewed as a failed trajectory. Similar to the Trajectory error, Location error (Loc. err.) is defined as the proportion of unsuccessful joints. In our experiments, we adopt 50cm as the distance threshold to calculate the Trajectory error and Location error. Average error (Avg. err.) denotes the mean distance between the joint positions in the generated motion and the given control trajectories.

C More Qualitative Results

In this section, we provide more qualitative results of our model. Fig. 5 illustrates the model’s generation results on the task of text-to-motion. All videos can be found on the project page.

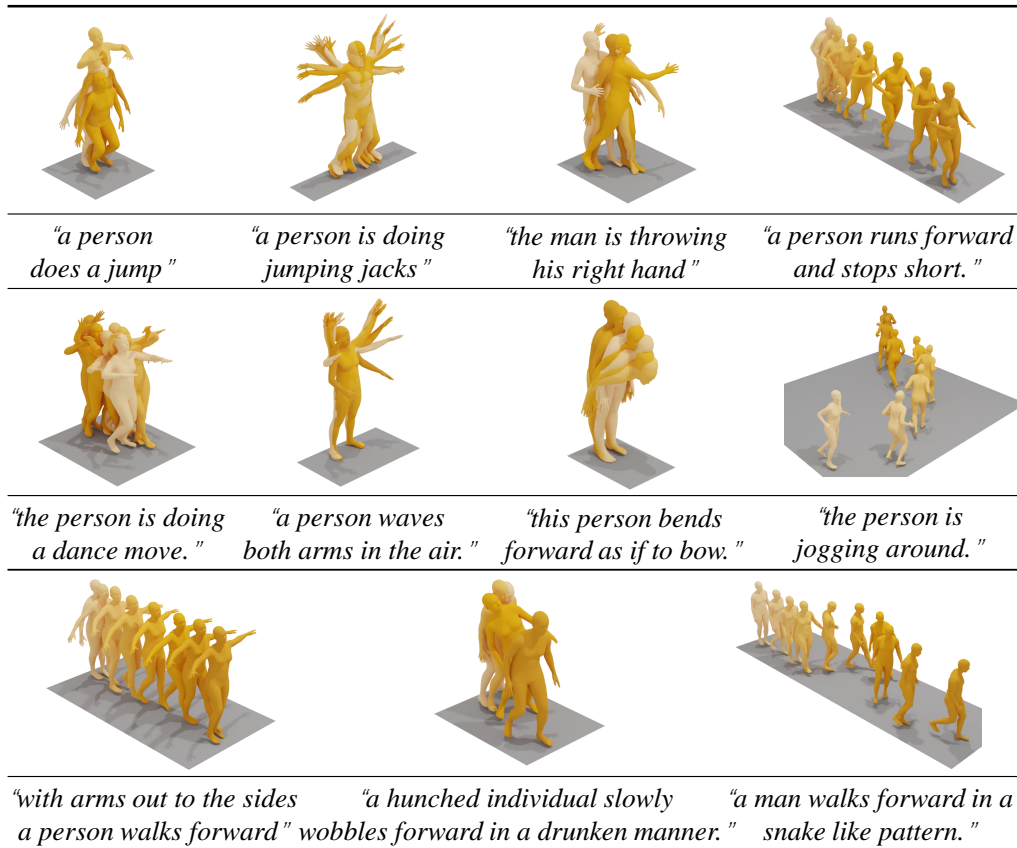


Figure 5: More qualitative results of MotionLCM on the task of text-to-motion.